

Ultraheavy diquark decaying into vectorlike quarks at the LHC

Ioana Duminica,^{1,2} Calin Alexa,¹ Ioan M. Dinu,¹ Bogdan Dobrescu,³ and Matei-Stefan Filip,^{1,2}

¹*IFIN-HH, Particle Physics Department, Măgurele, IF 077125, Romania*

²*University of Bucharest, Faculty of Physics, Măgurele, IF 077125, Romania*

³*Particle Theory Department, Fermilab, Batavia, IL 60510, USA*

(Dated: March 21, 2025)

We explore the discovery potential of ultraheavy (7 – 8.5 TeV) diquark scalars (S_{uu}) produced in the collision of two up quarks at the LHC. Assuming that the diquark scalar decays in two vectorlike quarks of mass around 2 TeV, each of them decaying into a W^+ boson and a b quark, we focus on the fully hadronic final state. We present a signal-from-background separation study based on a discriminator built with Machine Learning techniques. For this six-jet final state and a luminosity of 3000 fb^{-1} , we estimate that a diquark scalar of mass near 8 TeV may be discovered or ruled out even when its coupling to up quarks is as low as 0.2.

I. INTRODUCTION

Starting with the ongoing Run 3 data taking at the LHC and the upcoming high-luminosity LHC (HL-LHC) [1], explorations of physics near the 10 TeV scale become possible [2], and the discovery potential for physics beyond the Standard Model (SM) considerably increases, especially for ultraheavy particles near the kinematic limit of the collider.

In Run 2 of the LHC, the CMS Collaboration [3] observed two events with four hadronic jets characterized by very large tetrajet invariant mass M_{4j} , around 8 TeV. Moreover, in both events, the four jets are paired in two dijets, each having an invariant mass M_{2j} in the 1.9 – 2.1 TeV range. The QCD background for such events is of the order of 10^{-4} events [4], and the CMS Collaboration concluded that the two observed events constitute a 3.9σ excess over the SM prediction. Furthermore, CMS interpreted the excess in terms of a model presented in [4], in which a diquark scalar S_{uu} is produced in the s -channel from a uu initial state, and decays into a pair of vectorlike quarks χ . The subsequent decay $\chi \rightarrow ug$, which occurs at one loop [5], leads to events consistent with the observed $4j$ events provided S_{uu} and χ have masses $M_S \approx 8.5 \text{ TeV}$ and $m_\chi \approx 2.1 \text{ TeV}$, respectively.

A study similar to the CMS $4j$ search was performed by the ATLAS Collaboration [6]. An outlier 4-jet event with $M_{4j} \approx 6.6 \text{ TeV}$ was observed in that study, consisting of two dijets of $M_{2j} \approx 2.2 \text{ TeV}$ each. Although the 4-jet invariant mass of the ATLAS event is significantly below the ones of the CMS events, it is still consistent (roughly at the 1.5σ level) with the $uu \rightarrow S_{uu} \rightarrow \chi\chi \rightarrow 4j$ hypothesis employed by CMS, because the $4j$ invariant mass distribution produced by an ultraheavy S_{uu} has a long tail towards lower masses.

In this paper we study the LHC reach in a different possible final state of an ultraheavy S_{uu} , which arises from a more typical decay mode of the vectorlike quark χ , namely $S_{uu} \rightarrow \chi\chi \rightarrow (W^+b)(W^+b)$. The $\chi \rightarrow W^+b$ decay is unavoidable if there is mass mixing between χ and the SM top quark. An alternative origin of the $\chi \rightarrow$

W^+b decay may be a loop process, similar to the one responsible for $\chi \rightarrow ug$.

In either case, additional decay modes of χ are expected (such as Zt and h^0t ; the sum of these two branching fractions is approximately equal to the W^+b one in the case of mass mixing [7]), but they are more model dependent, and will be not be studied here.

We will focus mainly on hadronic final states of the W bosons arising from the χ decays, because these allow the reconstruction of the S_{uu} mass. Signal search optimization is done with Machine Learning (ML) methods, a powerful approach in particle and event identification and reconstruction largely used in multi-variable environments [8, 9].

In Section II we describe the interactions of the new particles, and the simulation of the signal and backgrounds. The ML discriminant is discussed in Section III, the selection efficiency is estimated in Section IV, and the S_{uu} observation potential is investigated in Section V. Our conclusions are presented in Section VI.

II. A DIQUARK AND A VECTORLIKE QUARK

The model considered here [2] (see also [4]) includes two particles beyond the SM: a diquark scalar, S_{uu} , and a vectorlike quark, χ . The S_{uu} diquark is a color-sextet weak-singlet complex scalar particle that carries electric charge $4/3$. The χ vectorlike quark is a color-triplet weak-singlet fermion that carries electric charge $2/3$.

The diquark has interactions with two up quarks, and also with two χ quarks, described by the following terms in the Lagrangian:

$$\frac{y_{uu}}{2} S_{uu} \bar{u}_R u_R^c + \frac{y_{\chi\chi}}{2} S_{uu} \bar{\chi}_R \chi_R^c + \text{H.c.} \quad (1)$$

Here the Yukawa couplings y_{uu} and $y_{\chi\chi}$ are parameters of order one, or smaller. The upper index c refers to charge conjugation, so that the Feynman rule associated with a Lagrangian term of the type $S_{uu} \bar{\chi}_R \chi_R^c$ is such that one

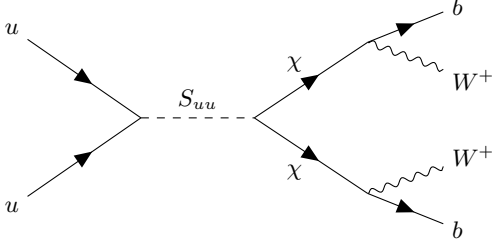


FIG. 1. Diquark S_{uu} production at the LHC, followed by a cascade decay through two vectorlike quarks. The final state is W^+bW^+b .

scalar enters the interaction vertex and two quarks exit from the vertex.

Other possible Yukawa interactions of S_{uu} , discussed in [2], are assumed here to have negligible couplings. The χ interaction with the W boson is taken to be

$$g_\chi W^+ \bar{\chi}_L \gamma^\mu b_L + \text{H.c.} , \quad (2)$$

where $g_\chi \ll 1$. This may arise, for example, from mass mixing between χ and the SM top quark [10]. Additional interactions of a single χ with a SM quark and a SM boson are expected, but their effects are taken into account here only indirectly, through a branching fraction $B(\chi \rightarrow Wb) < 1$.

The main production mechanism for S_{uu} at proton-proton colliders is from a uu initial state. Its subsequent decay into $\chi\chi$, followed by each χ decaying into W^+b , is represented by a single diagram, shown in Figure 1. The cross section for this $pp \rightarrow S_{uu} \rightarrow \chi\chi \rightarrow (W^+b)(W^+b)$ process, denoted here as $\sigma_s(WbWb)$, is given by

$$\sigma_s(WbWb) \approx \sigma_s(\chi\chi) B(\chi \rightarrow Wb)^2 , \quad (3)$$

where $\sigma_s(\chi\chi) \equiv \sigma(pp \rightarrow S_{uu} \rightarrow \chi\chi)$ is the production cross section for two χ quarks (not for $\chi\bar{\chi}$), which proceeds through an s -channel S_{uu} . Corrections due to similar processes with an off-shell χ are neglected here because the vectorlike quark is expected to have a very small decay width (but still sizable enough to allow prompt decays).

Four parameters control the characteristics of the $uu \rightarrow S_{uu} \rightarrow \chi\chi$ process: the M_S and m_χ masses, and the y_{uu} and $y_{\chi\chi}$ couplings introduced in Eq. (1). The branching fraction of the diquark into vectorlike quarks, $B(S_{uu} \rightarrow \chi\chi)$, is a function of the coupling ratio $y_{\chi\chi}/y_{uu}$ and of the mass ratio m_χ/M_S , and can be straightforwardly computed using the formulas for the $S_{uu} \rightarrow \chi\chi$ and $S_{uu} \rightarrow uu$ widths given in [5]. For example, when the ratios are $m_\chi/M_S = 1/4$ and $y_{\chi\chi}/y_{uu} = 1.5$, the branching fraction is $B(S_{uu} \rightarrow \chi\chi) \approx 63\%$.

The $\sigma_s(\chi\chi)$ cross section is approximately given by the product of the on-shell S_{uu} production cross section (computed in [4] based on the NLO formulas derived in [11]) times the branching fraction of the diquark: $\sigma_s(pp \rightarrow S_{uu}) B(S_{uu} \rightarrow \chi\chi)$. There are non-negligible effects due to off-shell S_{uu} exchange, but these

are relevant mostly for events with lower-energy final-state particles, where the backgrounds are larger. Note that $\sigma_s(pp \rightarrow S_{uu})$ is fast falling with increased M_S , and is proportional to y_{uu}^2 . Thus, from Eq. (3) it follows that $\sigma_s(WbWb)$ is approximately proportional to the square of $y_{uu} B(\chi \rightarrow Wb)$.

For ML discriminant (Section III) and signal selection efficiency studies (Section IV), we vary M_S in the 7–8.5 TeV range, and fix the χ mass and the coupling ratio at

$$m_\chi = 2 \text{ TeV} , \quad \frac{y_{\chi\chi}}{y_{uu}} = 1.5 . \quad (4)$$

We consider two values for the product of the S_{uu} coupling to up quarks with the branching fraction of χ :

$$y_{uu} B(\chi \rightarrow Wb) = 0.1, 0.2 . \quad (5)$$

Hence, for the typical value $B(\chi \rightarrow Wb) \approx 50\%$ [7, 10], the benchmark values for the coupling that we will consider here are $y_{uu} = 0.2$ and 0.4 .

The model described above, including the scalar diquark plus the vectorlike quark, was implemented in FeynRules [12], which outputs the MadGraph model files. For signal simulation we used MADGRAPH5_AMC@NLO [13] (v3.3.2) at leading order (LO) with the default PDF set (NNPDF23LO [14]), and the output interfaced to PYTHIA8.310 [15]. Detector response was simulated using DELPHES 3.5.0 [16] with both ATLAS and CMS parametrizations. Jets were reconstructed with FASTJET [17] using the anti- k_t algorithm [18].

In Figure 2 we show the $\sigma_s(\chi\chi)$ cross section computed with MadGraph as a function of M_S for $y_{uu} = 0.2$ (lower lines) and $y_{uu} = 0.4$ (upper lines); the values for other model parameters are fixed there as in Eq. (4). Signal and background data samples were generated at $\sqrt{s} = 13.6$ and 14 TeV without pileup.

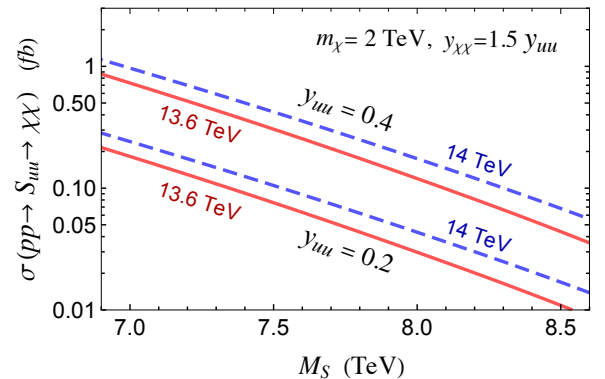


FIG. 2. Cross section for the $pp \rightarrow S_{uu} \rightarrow \chi\chi$ process as a function of the S_{uu} diquark mass, at center-of-mass energies of 13.6 TeV (solid red lines) and 14 TeV (dashed blue lines). This $\sigma_s(\chi\chi)$ is computed at LO with MadGraph [13] for two values of the S_{uu} coupling to up quarks: $y_{uu} = 0.2$ (bottom two lines) and 0.4 (top two lines). Other parameters are fixed as in Eq. (4).

For background simulation we use the following types of processes: $2 \rightarrow 2$ QCD, W +jets, Higgs processes, dibosons, and $t\bar{t}$; altogether there are 32 background processes [19]. For the signal selection relevant here, the most important background processes are $2 \rightarrow 2$ QCD, W +jets and dibosons. Due to the very high M_S values, we constrain the phase space for background simulation by imposing high values for the Pythia cut m_{HatMin} [15] (which represents the minimum invariant mass of the final state): $\hat{m}_{\min} \in [6, 8]$ TeV.

The signal considered here consists in two pairs of nearly collinear quark jets (originating from the two W^+ bosons) plus two b jets. Thus, besides the $2 \rightarrow 2$ QCD background included in our study, which is due to the showering of four extra jets, there are a few other QCD backgrounds that mimic our signal. These include the $2 \rightarrow k_j$ QCD processes with $k_j = 3, 4, 5$ and the showering of extra jets, as well as the $2 \rightarrow 6$ QCD processes. These additional QCD backgrounds, which we ignore, are difficult to simulate given the very large p_T associated with the signal produced by an ultraheavy S_{uu} ; nevertheless, we do not expect that they are substantially larger than the background due to $2 \rightarrow 2$ QCD plus showering, which is included simulated with Pythia.

III. MACHINE LEARNING DISCRIMINANT

Due to the complexity of the background relevant to this study, we decided to use Machine Learning algorithms to discriminate between signal and background rather than a cut-based analysis. We tested two ML classification models [20]: Boosted Decision Tree (BDT) [21] and Random Forest (RF) [22] (Neural Networks were also tested in a preliminary attempt [23]).

The BDT approach is the most commonly used for such classification tasks, relying on sequentially training multiple decision trees, where each new tree aims to correct the errors of the previous ones. Due to its fast training time, we choose the **XGBoost** [24] implementation of the BDT. In the case of the RF models, which also consist of ensembles of decision trees, the training is performed on different subsets of data and features. Their outputs are combined to make more accurate and robust predictions. Here, we use the **Scikit-learn** [25] implementation of the RF.

To obtain the ML discriminator, D , we input a selection of 75 variables into ML models: jet kinematics $p_T^{(i)}$, $\eta^{(i)}$, $\phi^{(i)}$, dijet angular distance $\Delta R^{(i,j)}$, dijet invariant mass $m_{2j}^{(i,j)}$, number of dijets N_{jj}^{W20} with $|m_{2j} - m_W| \leq 20$ GeV, max dijet p_T vector sum, max ΔR of any dijet pair, 3-jet invariant mass $m_{3j}^{(i,j,k)}$, jet multiplicity n_j , jet b -tag multiplicity and invariant mass $m_{2j}^{\Delta R^{\min}}$ of ΔR^{\min} dijet. To ensure consistency in the number of variables across events, as well as to leverage the power of the ML algorithm to find the best combination of variables, we consider all combinations for m_{2j} ,

m_{3j} and ΔR .

The classification of signal and background events is based on the trained ML model, which assigns to each event a probability score (P) with values ranging from 0 to 1. This score represents the likelihood that an event belongs to the signal category. To convert these continuous probability scores into discrete classifications, a series of thresholds or discriminator values (D), are applied. Events with $P > D$ are classified as signal, whereas those with $P \leq D$ are classified as background.

For this analysis, a wide range of discriminator values is considered, starting from 0.2, all the way to 0.99. These values allow for an evaluation of the model performance across different working points, with lower thresholds (*e.g.*, $D = 0.80$) classifying a larger number of events as signal, leading to higher signal efficiency but lower purity. In contrast, higher thresholds (*e.g.*, $D = 0.99$) result in a highly pure signal selection but at the cost of reduced efficiency. The signal and background distributions in the 0.20 – 0.80 discriminator range are uniform, so we have decided to present the results for $D \geq 0.80$. In order to maintain a good signal purity with a reasonable selection efficiency, we have set the higher boundary of the discriminant to $D = 0.97$.

To estimate the expected number of signal and background events, each event is weighted by its process-specific cross section, the total integrated luminosity, and the ratio of events passing the discriminator cut. We use the notation S_{ev} for the total number of expected signal events, while the background counts, denoted by B_{ev} , correspond to events that the model classifies as signal, regardless of their true origin (misclassified background events).

We simulated 10^5 events for each process, signal or background, of which 80% were used in training the models and the remaining 20% of the total sample was used for performance evaluation. In the following, we are showing the S_{ev} and B_{ev} values obtained for various cases. In Table I we present the number of events for signal and background obtained with BDT and RF for $D \geq 0.80$. Detector simulation is done here with the ATLAS parametrization of DELPHES [16], assuming

TABLE I. Number of events for signal (S_{ev}) and background (B_{ev}) obtained with the BDT and RF algorithms for the ATLAS detector parametrization at $\sqrt{s} = 13.6$ TeV and $\mathcal{L} = 3000 \text{ fb}^{-1}$, for $M_S = 7.5$ TeV, $y_{uu}B(\chi \rightarrow Wb) = 0.1$, and $\hat{m}_{\min} = 6$ TeV.

		$D=0.80$	$D=0.90$	$D=0.95$	$D=0.96$	$D=0.97$
BDT	S_{ev}	18.4	18.3	17.5	16.5	14.3
	B_{ev}	133	57.4	11.2	7.8	2.3
RF	S_{ev}	18.3	18.3	17.7	16.9	14.7
	B_{ev}	149	73.1	17.2	10.4	5.2

TABLE II. S_{ev} and B_{ev} obtained with RF for the CMS detector parametrization of Delphes. The parameters are fixed as specified in the caption of Table I.

	$D=0.80$	$D=0.90$	$D=0.95$	$D=0.96$	$D=0.97$
S_{ev}	18.3	18.3	17.7	16.9	14.7
B_{ev}	122.1	52.6	14.6	10.8	1.6

$\sqrt{s} = 13.6$ TeV, $\mathcal{L} = 3000 \text{ fb}^{-1}$, $M_S = 7.5$ TeV, and $y_{uu}B(\chi \rightarrow Wb) = 0.1$. The other model parameters are fixed as in Eq. (4), and the Pythia phase-space cut is set here at $\hat{m}_{\text{min}} = 6$ TeV.

From the results presented in Table I we can conclude that both ML classification models, RF and BDT, generally provide us with comparable results for the discriminator D in the interval $[0.80 - 0.97]$. However, depending on the random process of model parameter initialization, the BDT could end up with slightly smaller errors in some runs. Even so, we choose to continue our study with RF because it is less prone to over-fitting [26].

Table II shows S_{ev} and B_{ev} values obtained with the RF algorithm for the CMS parametrization of the Delphes detector simulation. Because we obtain similar signal-to-background discrimination for the CMS and ATLAS detector parametrizations (compare Tables II and I), in what follows we perform the signal selection efficiency study only for the ATLAS parametrization.

IV. SIGNAL SELECTION EFFICIENCY

In this Section we study how the number of signal and background events (S_{ev} and B_{ev}) depend on the RF and sample parameters. We first discuss the impact of variable weights on the ML discriminator D . Then, in Section IV B we compare S_{ev} and B_{ev} at two center-of-mass energies, $\sqrt{s} = 13.6$ TeV and 14 TeV, and investigate the relevance of the number of simulated events. In IV C, we explore the S_{ev} and B_{ev} dependence on the number of jets used by the ML algorithm, and we outline the influence of the phase-space cuts. All the studies of this Section are performed for $y_{uu}B(\chi \rightarrow Wb) = 0.1$, with other parameters fixed as in Eq. (4).

We use the k-fold cross-validation method to compute the errors of our ML algorithm. We work with 5 folds, splitting 10^5 events data sample into 80% for training and 20% for testing. In the case of S_{ev} we display only the mean values, but one should keep in mind that there are sizable uncertainties, especially from NLO effects and from PDFs at the large parton momentum fractions associated with an ultraheavy resonance. The errors on S_{ev} due to the ML algorithm are below 1%, so they are negligible compared to the uncertainties mentioned above.

For B_{ev} , in addition to the mean values, we display the errors due to the RF model performance as the standard deviation of all runs. We emphasize that there are

other large uncertainties on B_{ev} , for example from QCD processes (see Section II) not included in the simulation.

A. Feature importance

To gain insight into the decision-making process of the Random Forest classifier, we examine the feature importance scores assigned to each input variable. The importance of a feature is determined using the Mean Decrease in Impurity (MDI) method [27], which quantifies how much each feature contributes to improving the splits in the RF decision trees. Features that are more frequently used for splitting the data and lead to better separation between signal and background are assigned higher importance values. The final feature importance scores are averaged over all the decision trees in the RF and normalized to sum to one.

We run tests on different sample folds, center-of-mass energies, values of diquark mass M_S , values of the phase-space cut \hat{m}_{min} , number n_j of jets in the final state, and number N_{ev} of simulated events per process. Although distinct runs lead to distinguishable feature lists, they consist mainly of the same variables. Only slight changes between their ranking are observed. We have found that the transverse momentum of the fourth and the third final-state jets $p_{\text{T}}^{(4)}$ and $p_{\text{T}}^{(3)}$ are always the first two with importance score in the 12% – 14% range. Among the first 10 features, the following are always present: $m_{2j}^{(i,j)}$, $m_{2j}^{\Delta R^{\text{min}}}$, $p_{\text{T}}^{(2)}$ and $m_{3j}^{(i,j,k)}$. The importance score of each of these four kinematic variables is below 8%.

B. Center-of-mass energy and number of events

The increase in $\sigma_s(\chi\chi)$ cross-section with \sqrt{s} (as shown in Figure 2) translates into higher values of the number of signal events S_{ev} . At the same time, higher \sqrt{s} leads to a larger number of background events B_{ev} . Nevertheless, the six jets associated with the leading-order signal considered here have large transverse momenta, due to the very large mass of the s -channel resonance, so that the $S_{\text{ev}}/B_{\text{ev}}$ and $S_{\text{ev}}/\sqrt{B_{\text{ev}}}$ ratios grow with \sqrt{s} .

A comparison of the number of signal and background events for $\sqrt{s} = 13.6$ TeV versus $\sqrt{s} = 14$ TeV is presented in Table III, assuming an integrated luminosity $\mathcal{L} = 3000 \text{ fb}^{-1}$ in both cases. While the center-of-mass energy planned for the HL-LHC is 14 TeV, the current Run 3 of the LHC is at $\sqrt{s} = 13.6$ TeV. To be conservative, we will set $\sqrt{s} = 13.6$ TeV for our feasibility study. However, it should be emphasized that even a slightly larger center-of-mass energy (*e.g.*, 14 TeV) would increase the HL-LHC sensitivity to ultraheavy particles such as the diquark studied here.

Next, we analyze how the signal and background vary with the size of the simulated sample. In Table IV we show S_{ev} and B_{ev} obtained for different number N_{ev} of

TABLE III. Number of events for signal (S_{ev}) and background (B_{ev}) obtained for two center-of-mass energies, 13.6 TeV and 14 TeV, with 3000 fb^{-1} of simulated data, when $M_S = 7.5 \text{ TeV}$, $\hat{m}_{min} = 6 \text{ TeV}$, and $y_{uu}B(\chi \rightarrow Wb) = 0.1$. Other model parameters are fixed as in Eq. (4).

	$D = 0.80$	$D = 0.90$	$D = 0.95$	$D = 0.96$	$D = 0.97$
$\sqrt{s} = 13.6 \text{ TeV}$					
S_{ev}	18.3	18.3	17.7	16.9	14.7
B_{ev}	149 ± 21	73.1 ± 11.4	17.2 ± 4.0	10.4 ± 0.6	5.2 ± 2.9
$\sqrt{s} = 14 \text{ TeV}$					
S_{ev}	25.3	25.3	24.4	23.3	20.3
B_{ev}	209 ± 9	113 ± 5	21.8 ± 7.2	14.7 ± 6.8	3.1 ± 2.4

TABLE IV. S_{ev} and B_{ev} dependence on the number of simulated events per process at $\sqrt{s} = 13.6 \text{ TeV}$ and $\mathcal{L} = 3000 \text{ fb}^{-1}$, for $M_S = 7.5 \text{ TeV}$ and other parameters as in Table III. The uncertainties for B_{ev} displayed here are only due to the errors of the ML algorithm (same type of errors for S_{ev} are below 1%).

	$D = 0.80$	$D = 0.90$	$D = 0.95$	$D = 0.96$	$D = 0.97$
$N_{ev} = 10^5$					
S_{ev}	18.3	18.3	17.7	16.9	14.7
B_{ev}	149 ± 21	73.1 ± 11.4	17.2 ± 4.0	10.4 ± 0.6	5.2 ± 2.9
$N_{ev} = 2 \times 10^5$					
S_{ev}	18.3	18.3	17.7	17.0	14.8
B_{ev}	139 ± 9	71.0 ± 8.5	17.5 ± 3.8	8.2 ± 3.7	3.1 ± 1.4
$N_{ev} = 3 \times 10^5$					
S_{ev}	18.3	18.3	17.8	17.0	14.9
B_{ev}	133 ± 11	71.9 ± 6.3	17.1 ± 3.9	7.9 ± 2.8	2.7 ± 1.4

simulated events. When the number N_{ev} of MC simulated events per process varies from $N_{ev} = 10^5$ to $N_{ev} = 3 \times 10^5$ and $D \leq 0.97$, we see that the number of background events is getting smaller for a fixed discriminator (D) value. However, for a fixed value of D , the S_{ev} variation between samples is almost negligible. Although the signal-to-background selection is slightly improved for $N_{ev} = 3 \times 10^5$ compared to $N_{ev} = 10^5$, we have decided to continue our study with $N_{ev} = 10^5$ samples in order to gain computational efficiency.

C. Number of jets and phase-space cut

The final state arising from the cascade decay of the S_{uu} scalar into $(W^+b)(W^+b)$, with hadronic W^+ decays, consists in two pairs of nearly collinear quark jets and two b jets. Even though this signal process involves a 6-jet final state, additional jets are produced in the same event due to multiparton interactions, and parton show-

TABLE V. S_{ev} and B_{ev} for a few choices of the number of final state jets taken into account by the ML algorithm at $\sqrt{s} = 13.6 \text{ TeV}$ and $\mathcal{L} = 3000 \text{ fb}^{-1}$, for $M_S = 7.5 \text{ TeV}$ and $\hat{m}_{min} = 7 \text{ TeV}$.

	$D = 0.80$	$D = 0.90$	$D = 0.95$	$D = 0.96$	$D = 0.97$
$n_j = 4$					
S_{ev}	18.3	18.3	18.0	17.6	16.0
B_{ev}	11.9 ± 0.3	11.9 ± 0.3	1.9 ± 0.7	1.0 ± 0.4	0.34 ± 0.20
$n_j = 6$					
S_{ev}	18.3	18.3	18.0	17.6	16.0
B_{ev}	15.0 ± 1.3	8.0 ± 4.6	2.03 ± 0.80	1.1 ± 0.5	0.18 ± 0.05
$n_j = 8$					
S_{ev}	18.3	18.3	18.1	17.6	16.1
B_{ev}	18.9 ± 1.7	6.46 ± 1.49	2.08 ± 0.62	1.2 ± 0.6	0.17 ± 0.07

ering. Notice that initial- and final-state radiation also contribute additional jets, but these are NLO effects, and are not taken into account in this analysis.

In some events, the number of jets may be smaller due to possible collimation between some jets. In particular, each of the two W^+ bosons from the final state is typically boosted due to the large S_{uu} mass. Thus, each W^+ often produces a single jet with a two-prong substructure.

After the jets are ordered according to their transverse momentum, the ML algorithm takes into account a number n_j of jets with highest p_T . As shown in Table V, the number of signal events (S_{ev}) has only a very weak dependence on n_j , which is negligible within errors. For $D \leq 0.95$, we observe a better signal versus background discrimination for the $n_j = 4$ case than for the other ones. When increasing the number of jets to $n_j = 6$ and $n_j = 8$, signal-to-background selection becomes comparable. Due to this finding we have decided to continue the current study with the first six most energetic jets taken into account by the ML algorithm.

The background simulation employed here strongly depends on the phase-space cut \hat{m}_{min} . In Figure 3 we show that B_{ev} values (at $\mathcal{L} = 3000 \text{ fb}^{-1}$) decrease for higher phase-space cuts \hat{m}_{min} , which means better performance of the ML algorithm. Table VI shows the S_{ev} and B_{ev} values for a fixed diquark scalar mass and different \hat{m}_{min} . The highest number of signal events and the lowest number of background events are obtained for the highest phase-space cut.

V. S_{uu} OBSERVATION POTENTIAL

The purpose of this study is to investigate the discovery potential of a heavy diquark scalar S_{uu} which decays into a pair of vectorlike quarks, as described by the model presented in [2]. CMS Collaboration [3] observed two events with four hadronic jets that form a very large invariant

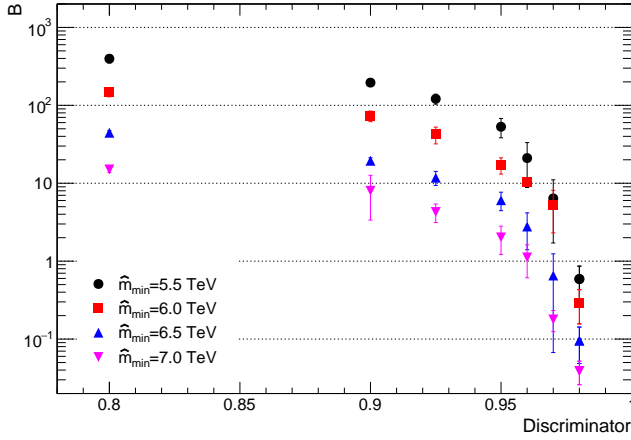


FIG. 3. Number of background events (B_{ev}) as a function of discriminator D , for different values of the phase-space cut (\hat{m}_{min}). The integrated luminosity is taken to be $\mathcal{L} = 3000 \text{ fb}^{-1}$ at $\sqrt{s} = 13.6 \text{ TeV}$ and the diquark mass is fixed at $M_S = 7.5 \text{ TeV}$.

TABLE VI. S_{ev} and B_{ev} for different choices of the Pythia phase-space cut \hat{m}_{min} for $M_S = 7.5 \text{ TeV}$ and other parameters fixed as in Table IV.

	$D = 0.80$	$D = 0.90$	$D = 0.95$	$D = 0.96$	$D = 0.97$
$\hat{m}_{\text{min}} = 5.5 \text{ TeV}$					
S_{ev}	18.3	18.3	17.8	17.0	14.8
B_{ev}	397 ± 46	196 ± 19	53.1 ± 14.8	21.0 ± 12.2	6.4 ± 4.7
$\hat{m}_{\text{min}} = 6 \text{ TeV}$					
S_{ev}	18.3	18.3	17.7	16.9	14.7
B_{ev}	149 ± 21	73.1 ± 11.4	17.2 ± 4.0	10.4 ± 0.6	5.2 ± 2.9
$\hat{m}_{\text{min}} = 6.5 \text{ TeV}$					
S_{ev}	18.3	18.3	17.8	17.1	15.1
B_{ev}	44.4 ± 2.9	19.4 ± 1.8	6.1 ± 1.6	2.8 ± 1.4	0.65 ± 0.59
$\hat{m}_{\text{min}} = 7 \text{ TeV}$					
S_{ev}	18.3	18.3	18.0	17.6	16.0
B_{ev}	15.0 ± 1.3	8.0 ± 4.6	2.0 ± 0.8	1.1 ± 0.5	0.18 ± 0.05

mass M_{4j} , around 8 TeV, and are paired in two dijets, each having an invariant mass M_{2j} near 2 TeV. While the ATLAS search [6] in the same final state yielded no events with M_{4j} at 8 TeV, it reported an intriguing event with $M_{4j} \approx 6.6 \text{ TeV}$ that appears consistent with a pair-produced vectorlike quark of mass near 2 TeV.

This motivates our choice of the masses for the new particles, M_S in the 7–8.5 TeV range, and $m_\chi \approx 2 \text{ TeV}$. Even if the events mentioned above could turn out to be just a very unlikely fluctuation of the QCD background, the search for resonantly produced vectorlike quarks discussed here is a well-motivated exploration of physics at

TABLE VII. Number of signal events $S_{\text{ev}}(0.1)$ and $S_{\text{ev}}(0.2)$, for $y_{uu}B(\chi \rightarrow Wb) = 0.1$ and 0.2, respectively, number of background events B_{ev} , predicted for different values of the diquark mass, with 3000 fb^{-1} of data at $\sqrt{s} = 13.6 \text{ TeV}$, and a phase-space cut $\hat{m}_{\text{min}} = M_S - 0.5 \text{ TeV}$.

	$D = 0.80$	$D = 0.90$	$D = 0.95$	$D = 0.96$	$D = 0.97$
$M_S = 7.0 \text{ TeV}$					
$S_{\text{ev}}(0.1)$	43.9	43.8	43.0	41.9	37.9
$S_{\text{ev}}(0.2)$	197	196	193	188	170
B_{ev}	42.4	17.9	5.05	3.96	0.79
$M_S = 7.5 \text{ TeV}$					
$S_{\text{ev}}(0.1)$	18.3	18.3	18.0	17.6	16.0
$S_{\text{ev}}(0.2)$	81.9	81.8	80.5	78.6	71.5
B_{ev}	15.0	8.00	2.03	1.12	0.18
$M_S = 8.0 \text{ TeV}$					
$S_{\text{ev}}(0.1)$	7.20	7.20	7.10	6.95	6.35
$S_{\text{ev}}(0.2)$	32.4	32.4	31.9	31.3	28.5
B_{ev}	5.34	5.34	0.67	0.36	0.09
$M_S = 8.5 \text{ TeV}$					
$S_{\text{ev}}(0.1)$	2.63	2.63	2.59	2.54	2.33
$S_{\text{ev}}(0.2)$	11.8	11.8	11.6	11.4	10.5
B_{ev}	1.72	1.72	0.17	0.09	0.02

scales in the multi-TeV range.

We present here our results regarding the observation potential of the ultraheavy diquark scalar S_{uu} , obtained with 3000 fb^{-1} of simulated data at $\sqrt{s} = 13.6 \text{ TeV}$ based on a sliding phase-space cut given by $\hat{m}_{\text{min}} = M_S - 0.5 \text{ TeV}$. The number of signal and background events shown in Table VII corresponds to different values of M_S . The signal is shown there for two values of the dimensionless parameter $y_{uu}B(\chi \rightarrow Wb)$: 0.1 and 0.2, with the number of signal events labeled by $S_{\text{ev}}(0.1)$ and $S_{\text{ev}}(0.2)$, respectively. Because this observation potential study relies on an incomplete simulation of the background, and uses the DELPHES detector simulation [16], which has larger uncertainties compared to full detector simulations, the k-fold cross-validation errors of the RF are not included in Table VII.

For $y_{uu}B(\chi \rightarrow Wb) = 0.1$ and $M_S = 8 \text{ TeV}$ the 95% upper limit of our background estimate is about 0.4 events when the discriminator is $D = 0.96$. At this point in parameter space of the model with S_{uu} and χ , the expected number of events is $S_{\text{ev}}(0.1) + B_{\text{ev}} \approx 7.3$. The probability for the SM background to have a large upward fluctuation such that 7 or more events are observed, in the absence of a new physics signal, can be computed using Poisson statistics (for an analysis of potential complications, see [28]) and is given by 1.1×10^{-7} . This is slightly above a 5σ excess, and can be considered a discovery.

The large uncertainties in the background may degrade

the significance of the excess, but when the discriminator is increased to $D = 0.97$ the background decreases by a factor of four while the signal decreases only by about 10%. Even if B_{ev} were 0.25 events (which is almost three times larger than the estimate background at $D = 0.97$ and $M_S = 8$ TeV), its fluctuation into 6 or more observed events would have a probability of only 2.7×10^{-7} . In that case the new physics model discussed here, which predicts $S_{\text{ev}}(0.1) + B_{\text{ev}} \approx 6.6$, would be again favored over the SM at the 5σ level.

Based on these results, we conclude that our ML method provides a good HL-LHC discovery potential for an S_{uu} of mass near 8 TeV, which decays into $(W^+b)(W^+b)$ with a final state consisting of six jets, provided $y_{uu}B(\chi \rightarrow Wb) \geq 0.1$. Given that the typical branching fraction of a vectorlike quark that mixes with the top quark is $B(\chi \rightarrow Wb) \approx 50\%$, the signal discussed here can be discovered even when y_{uu} is as small as 0.2.

For a heavier S_{uu} , with mass near 8.5 TeV, a larger y_{uu} may be necessary for discovery. As can be seen from Table VII, a factor of 2 increase in y_{uu} is already sufficient for discovery at $M_S = 8.5$ TeV, as it would lead to about 11 signal events, while the background is below 0.2 events for an ML discriminator $D \geq 0.95$.

Existing ATLAS [29] and CMS [30] searches for vectorlike quarks (which set lower mass limits on χ in the 1.4 – 1.7 TeV range), which include $(W^+b)(W^-\bar{b})$ final states, are not well-suited for setting limits on the resonantly produced $\chi\chi$ signal discussed here because the ultraheavy S_{uu} diquark forces the vectorlike quarks to be boosted, changing substantially the kinematic distributions of the final states. Likewise, existing ATLAS [31] and CMS [32] searches for 6-jets final states do not take advantage of the large p_T 's of the jets originating from a cascade decay of an ultraheavy s -channel resonance. Thus, it is important that the experimental collaborations perform dedicated searches for the signal analyzed here.

We emphasize that in this work we focused only on the fully-hadronic final state arising from the $pp \rightarrow S_{uu} \rightarrow \chi\chi \rightarrow (W^+b)(W^+b)$ process. Semileptonic and fully leptonic final states of the W^+ pair may be included to increase the sensitivity of the searches in the $(W^+b)(W^+\bar{b})$ final states. Furthermore, as mentioned in [2], the sensitivity to an ultraheavy S_{uu} may be improved by taking into account other decay modes of χ , for example into tZ and th^0 .

VI. CONCLUSIONS

We studied the discovery potential of LHC experiments for resonantly produced vectorlike quarks, in the case where the s -channel resonance is a diquark scalar particle, S_{uu} , with mass in the 7 – 8.5 TeV range. Such an ultraheavy particle may be produced with a sufficiently large cross section at the LHC because it has a coupling to two up quarks, and thus benefits from the largest PDF near the kinematic limit of the collider.

Previous studies of resonantly produced vectorlike quarks [4, 5] considered their exotic decay into two jets, motivated by the CMS observation of two remarkable events with $M_{4j} \approx 8$ TeV. Here we analyzed the more standard decay of a charged-2/3 vectorlike quark into W^+b , which is often expected to have the largest branching fraction (based on the assumption that mass mixing with the top quark is sufficiently large [7]).

Given that the S_{uu} resonance can be reconstructed when both W^+ bosons decay hadronically, in this paper we focused on the 6-jet final state arising from the $pp \rightarrow S_{uu} \rightarrow \chi\chi \rightarrow (W^+b)(W^+b)$ process. For the signal selection study we used Machine Learning models trained to discriminate against background sources. In particular, we investigated the impact of the variables weight, centre-of-mass energy, MC sample size, final state jet multiplicity, phase space selection, and diquark scalar mass on the Random Forest Machine Learning algorithm performance.

Our results indicate that searches at ATLAS or CMS in the above 6-jet final state with a luminosity of 3000 fb^{-1} may discover or rule out a diquark scalar of mass near 8 TeV even when its coupling to up quarks is as small as $y_{uu} \approx 0.2$. This is a promising result for the scientific impact of future searches at the HL-LHC in this channel. Furthermore, it is likely that the ATLAS and CMS experimental collaborations would obtain more precise results using their own simulation framework, and may use additional features of the proposed signal to improve the sensitivity of future searches for resonantly produced vectorlike quarks.

Acknowledgments: We thank Ethan Caninaert, John Conway, Patrick Fox, Robert Harris and Julien Maurer for valuable comments and suggestions. The work of I.D., C.A., I.-M.D. and M.-S.F. was supported by IFIN-HH under Contract No. PN-23210104 with the Romanian Ministry of Education and Research. The work of B.D. was supported by Fermi Forward Discovery Group, LLC under Contract No. 89243024CSC000002 with the U.S. Department of Energy, Office of Science, Office of High Energy Physics.

[1] I. Zurbano Fernandez *et al.*, High-Luminosity Large Hadron Collider (HL-LHC): Technical design report **10/2020**, 10.23731/CYRM-2020-0010 (2020).

[2] B. A. Dobrescu, LHC probes of the 10 TeV scale (2019), arXiv:1912.13155 [hep-ph].

[3] A. Tumasyan *et al.* (CMS), Search for resonant and

- nonresonant production of pairs of dijet resonances in proton-proton collisions at $\sqrt{s} = 13$ TeV, JHEP **07**, 161 (2023), arXiv:2206.09997 [hep-ex].
- [4] B. A. Dobrescu, R. M. Harris, and J. Isaacson, Ultra-heavy resonances at the LHC: beyond the QCD background (2018), arXiv:1810.09429 [hep-ph].
 - [5] B. A. Dobrescu, TeV-scale particles and LHC events with dijet pairs (2024), arXiv:2411.04121 [hep-ph].
 - [6] G. Aad *et al.* (ATLAS), Pursuit of paired dijet resonances in the Run 2 dataset with ATLAS, Phys. Rev. D **108**, 112005 (2023), arXiv:2307.14944 [hep-ex].
 - [7] T. Han, H. E. Logan, B. McElrath, and L.-T. Wang, Phenomenology of the little Higgs model, Phys. Rev. D **67**, 095004 (2003), arXiv:hep-ph/0301040.
 - [8] X. C. Vidal, L. D. Maroñas, and A. D. Suárez, How to Use Machine Learning to Improve the Discrimination between Signal and Background at Particle Colliders, Appl. Sciences **11**, 11076 (2021), arXiv:2110.15099 [hep-ex].
 - [9] K. Albertsson *et al.*, Machine Learning in High Energy Physics Community White Paper, J. Phys. Conf. Ser. **1085**, 022008 (2018), arXiv:1807.02876 [physics.comp-ph].
 - [10] B. A. Dobrescu, K. Kong, and R. Mahbubani, Prospects for top-prime quark discovery at the Tevatron, JHEP **06**, 001 (2009), arXiv:0902.0792 [hep-ph].
 - [11] T. Han, I. Lewis, and T. McElmurry, QCD Corrections to Scalar Diquark Production at Hadron Colliders, JHEP **01**, 123 (2010), arXiv:0909.2666 [hep-ph].
 - [12] A. Alloul, N. D. Christensen, C. Degrande, C. Duhr, and B. Fuks, FeynRules 2.0 - A complete toolbox for tree-level phenomenology, Comput. Phys. Commun. **185**, 2250 (2014), arXiv:1310.1921 [hep-ph].
 - [13] J. Alwall, R. Frederix, S. Frixione, V. Hirschi, F. Maltoni, O. Mattelaer, H. S. Shao, T. Stelzer, P. Torrielli, and M. Zaro, The automated computation of tree-level and next-to-leading order differential cross sections, and their matching to parton shower simulations, JHEP **07**, 079 (2014), arXiv:1405.0301 [hep-ph].
 - [14] R. D. Ball *et al.* (NNPDF), Parton distributions for the LHC Run II, JHEP **04**, 040 (2015), arXiv:1410.8849 [hep-ph].
 - [15] C. Bierlich *et al.*, A comprehensive guide to the physics and usage of PYTHIA 8.3, SciPost Phys. Codeb. **2022**, 8 (2022), arXiv:2203.11601 [hep-ph].
 - [16] J. de Favereau, C. Delaere, P. Demin, A. Giammanco, V. Lemaitre, A. Mertens, and M. Selvaggi (DELPHES 3), DELPHES 3, A modular framework for fast simulation of a generic collider experiment, JHEP **02**, 057 (2014), arXiv:1307.6346 [hep-ex].
 - [17] M. Cacciari, G. P. Salam, and G. Soyez, FastJet User Manual, Eur. Phys. J. C **72**, 1896 (2012), arXiv:1111.6097 [hep-ph].
 - [18] M. Cacciari, G. P. Salam, and G. Soyez, The anti- k_t jet clustering algorithm, JHEP **04**, 063 (2008), arXiv:0802.1189 [hep-ph].
 - [19] I.-M. Dinu, Diquark Simulation <https://github.com/imdinu/diquark-simulation/tree/main/hadronic/cards>, GitHub (2023).
 - [20] I.-M. Dinu, Diquark Analysis <https://github.com/imdinu/diquark-analysis>, GitHub (2023).
 - [21] J. H. Friedman, Greedy function approximation: A gradient boosting machine., Annals Statist. **29**, 1189 (2001).
 - [22] T. K. Ho, Random decision forests, in *Proceedings of 3rd International Conference on Document Analysis and Recognition*, Vol. 1 (1995) pp. 278–282 vol.1.
 - [23] I. Duminica, I.-M. Dinu, A. Jinaru, B. Dobrescu, and C. Alexa, Resonant production of vectorlike quarks at the HL-LHC, PoS **ICHEP2024**, 308 (2025).
 - [24] T. Chen and C. Guestrin, XGBoost: A scalable tree boosting system, in *Proceedings of the 22nd ACM SIGKDD International Conference on Knowledge Discovery and Data Mining*, KDD '16 (ACM, New York, NY, USA, 2016) pp. 785–794.
 - [25] F. Pedregosa *et al.*, Scikit-learn: Machine Learning in Python, Journal of Machine Learning Research **12**, 2825 (2011).
 - [26] T. Hastie, R. Tibshirani, and J. Friedman, *The Elements of Statistical Learning: Data Mining, Inference, and Prediction*, Springer series in statistics (Springer, 2009).
 - [27] L. Breiman, J. Friedman, C. Stone, and R. Olshen, *Classification and Regression Trees* (Taylor & Francis, 1984).
 - [28] G. J. Feldman and R. D. Cousins, A Unified approach to the classical statistical analysis of small signals, Phys. Rev. D **57**, 3873 (1998), arXiv:physics/9711021.
 - [29] G. Aad *et al.* (ATLAS), Search for pair-production of vector-like quarks in lepton+jets final states containing at least one b-tagged jet using the Run 2 data from the ATLAS experiment, Phys. Lett. B **854**, 138743 (2024), arXiv:2401.17165 [hep-ex].
 - [30] A. Tumasyan *et al.* (CMS), Search for pair production of vector-like quarks in leptonic final states in proton-proton collisions at $\sqrt{s} = 13$ TeV, JHEP **07**, 020 (2023), arXiv:2209.07327 [hep-ex].
 - [31] G. Aad *et al.* (ATLAS), A search for R-parity-violating supersymmetry in final states containing many jets in pp collisions at $\sqrt{s} = 13$ TeV with the ATLAS detector, JHEP **05**, 003 (2024), arXiv:2401.16333 [hep-ex].
 - [32] A. Hayrapetyan *et al.* (CMS), Searches for Pair-Produced Multijet Resonances Using Data Scouting in Proton-Proton Collisions at $\sqrt{s} = 13$ TeV, Phys. Rev. Lett. **133**, 201803 (2024), arXiv:2404.02992 [hep-ex].